

Pressure dependence of electron-phonon coupling in Ce^{3+} -doped $\text{Gd}_3\text{Sc}_2\text{Al}_3\text{O}_{12}$ garnet crystals

M. Grinberg and J. Barzowska

Institute of Experimental Physics, University of Gdańsk, Wita Stwosza 57, 80-952 Gdańsk, Poland

YongRong Shen

Department of Physics and High Pressure Science and Engineering Center, University of Nevada Las Vegas, Las Vegas, Nevada 89154-4002, USA

Richard S. Meltzer and Kevin L. Bray

Department of Physics and Astronomy, University of Georgia, Athens, Georgia 30602-2451, USA

(Received 5 December 2003; revised manuscript received 25 February 2004; published 5 May 2004)

Spectroscopic properties of Ce^{3+} in $\text{Gd}_3\text{Sc}_2\text{Al}_3\text{O}_{12}$ have been investigated by high-pressure luminescence and absorption spectroscopy up to 200 kbar. The emission and absorption bands originating from $5d \leftrightarrow 4f$ transitions were observed to shift to red with pressure at a rate of $-7.9 \text{ cm}^{-1}/\text{kbar}$ and $-15.2 \text{ cm}^{-1}/\text{kbar}$, respectively. A large difference in the pressure-induced shifts indicates a large decrease in the electron-lattice coupling strength. Using the standard crystal-field approach and configurational coordinate model, quantitative descriptions of the effect of pressure on the energy, band shape, and electron-phonon coupling have been conducted. We have found that the local compression of a $[\text{CeO}_8]^{13-}$ complex in $\text{Gd}_3\text{Sc}_2\text{Al}_3\text{O}_{12}:\text{Ce}^{3+}$ is about two times smaller than that of bulk material. We have also estimated the local Grüneisen parameter for $\text{Gd}_3\text{Sc}_2\text{Al}_3\text{O}_{12}:\text{Ce}^{3+}$ system to be about 2.66.

DOI: 10.1103/PhysRevB.69.205101

PACS number(s): 78.55.Hx, 71.70.-d, 62.50.+p, 76.30.Kg

I. INTRODUCTION

Garnet crystals doped with rare-earth ions such as Nd^{3+} , Er^{3+} , Ce^{3+} are extensively investigated and have found many applications in areas such as solid state lasers,¹ optical communications, scintillation,²⁻⁴ medical procedures, imaging, displays, flow cytometry, holography, and remote sensing.⁵⁻⁷ In particular, since Ce^{3+} is a dopant that has a lower $5d$ state from which it can emit from the near ultraviolet to the visible, it produces new applications such as tunable solid-state lasers over a wide spectral range.

It is known that Ce^{3+} ions in the garnet host occupy dodecahedral sites. The $4f$ ground electronic configuration splits, due to the spin-orbit interaction, into two states (${}^2F_{5/2}$ and ${}^2F_{7/2}$) with a splitting energy of about 2000 cm^{-1} . The emitting state of Ce^{3+} is the lowest orbital component [$5d(1)$] of the excited $5d$ electronic configuration. Since the electron-lattice interaction is much stronger in the $5d$ excited state than that in the $4f$ ground state a tenfold degeneracy of the $5d$ excited state is removed partially by crystal fields, whereas the influence of the crystal field on the $4f$ states is negligible. The energy of the $5d(1)$ emitting state of Ce^{3+} in crystal is diminished relative to its free-ion state by amount called as the depression energy (E_{depr}),³ given by

$$E_{depr} = -E_{cr} + E_{cen}, \quad (1)$$

where E_{cen} is the $5d$ centroid shift, measuring the redshift for the $5d$ barycenter relative to the free-ion state due to the nephelauxetic effect associated with the surrounding ligands and E_{cr} is the energy of crystal field. In a cubic crystal-field environment, the crystal-field energy is simply given by $E_{cr} = (16/3)Dq$, where Dq is the crystal-field strength. Since Ce^{3+} in the garnet lattice is at a distorted dodecahedral site,

described by a point group D_2 , the $5d(1)$ state is further split and the simple cubic approximation cannot be used more reasonably to describe the crystal-field effects such as splittings. However, at our present point, the cubic crystal-field approximation is still used reasonably to describe a pressure-induced change in E_{cr} and leads to $E_{cr} \propto Q^{-5}$ (because $Dq \propto Q^{-5}$), where Q is the configurational coordinate that is proportional to the average distance between Ce^{3+} and O^{2-} in the lattice.⁸ The $5d$ centroid shift E_{cen} is proportional to Q^{-6} according to the ligand polarization model.⁹ Figure 1(a) schematically shows the energetic structure of the $5d$ state of Ce^{3+} .

The next important effect that strongly modifies the energetic structure of the $5d$ excited state is the electron-lattice interaction that can be described by the configurational coordinate model in many material systems [Fig. 1(b)].¹⁰ The energy of the $5d(1)$ emitting state is additionally lowered by an amount of $S\hbar\omega$, where $\hbar\omega$ is the average energy of local phonon modes around Ce^{3+} and S is the Huang-Rhys factor.

In a successful scintillating application of Ce^{3+} -doped materials, a process of energy transfer from band-band excitations to $4f \rightarrow 5d$ excitations is a governing factor in useful scintillators. This process becomes efficient only if the $5d(1)$ emitting state of Ce^{3+} is energetically well separated from the band edges to avoid the occurrence of nonradiative processes in the emitting state via a back transfer to the host lattice. It is known that when the $5d(1)$ emitting state is resonant with the conduction band of the host lattice, it can be depopulated due to conversion of the excitation energy into mobile charges.¹¹ This reduces the luminescence efficiency of Ce^{3+} . Since the energetical location of the $5d(1)$ emitting state of Ce^{3+} relative to the band edge of the lattice is considerably influenced by crystal fields and electron-phonon interactions with neighboring ions, a quantitative un-

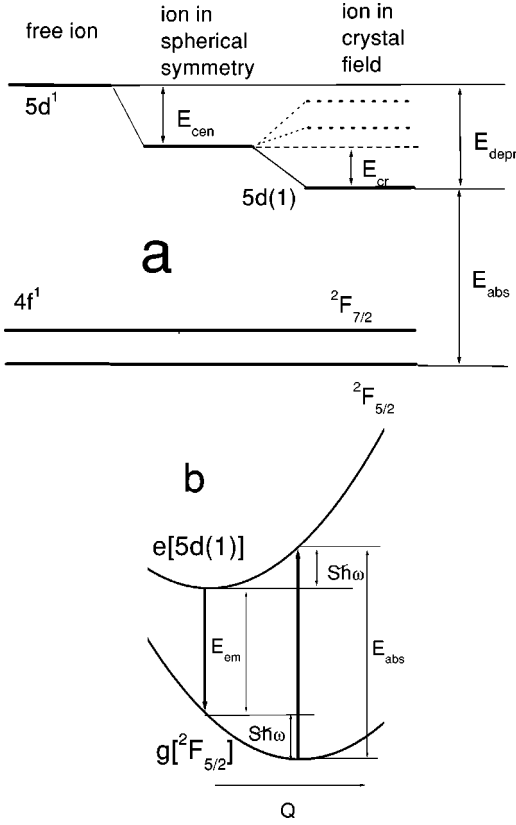


FIG. 1. A simplified energy diagram (a) and a configurational coordinate diagram (b) for Ce^{3+} in a host lattice.

Understanding of those interactions in Ce^{3+} systems is essential for improving the efficiency in Ce^{3+} -related scintillators.

In this paper, we present the results of our high-pressure emission and absorption investigation on $\text{Gd}_3\text{Sc}_2\text{Al}_3\text{O}_{12}:\text{Ce}^{3+}$ (GSAG: Ce^{3+}) up to 200 kbar. The results are discussed and compared with a prior high-pressure luminescence study in $\text{Y}_3\text{Al}_5\text{O}_{12}:\text{Ce}^{3+}$ (YAG: Ce^{3+}) system.¹² The major purpose of our present study is to analyze the influence of pressure on electron-lattice interactions in the $5d(1)$ excited state and to generalize a model that describes the interaction of the $5d$ states of Ce^{3+} with garnet host lattices.

II. EXPERIMENTS AND RESULTS

Garnet crystals were grown by the Czochralski method. The GSAG: Ce^{3+} samples contained Ce^{3+} concentrations of 0.33, 1, and 3.3%.

High pressure was applied to the sample using a Merrill-Bassett-type diamond anvil cell. A silicone (dimethylsiloxane) fluid was used as a pressure-transmitting medium and remained quasihydrostatic in our present pressure range.¹³ The standard ruby fluorescence technique was used for pressure determination. The Ce^{3+} luminescence was excited with a 488.0 nm argon laser line. The absorption spectra were measured with an optical microscope equipped with a charge-coupled device (CCD) camera.

All the observed luminescence spectra were corrected for

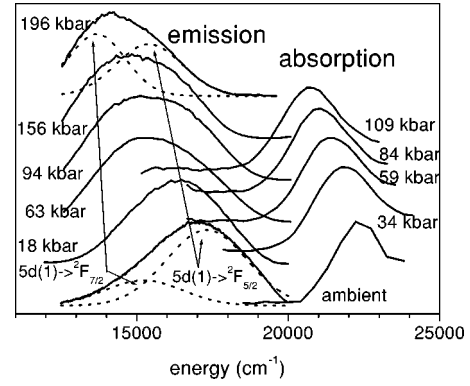


FIG. 2. Typical room-temperature absorption and emission spectra of GSAG: Ce^{3+} at several pressures. Dashed curves represent the fitted Gaussian functions for the $5d(1) \rightarrow {}^2F_{5/2}$ and $5d(1) \rightarrow {}^2F_{7/2}$ emission bands.

the instrumental response and presented in a line shape versus energy form in which the spectral line shape (L) as a function of energy ($\hbar\Omega$) $L(\hbar\Omega) \propto I(\hbar\Omega)[\hbar\Omega]^{-3}$. In the same approach, the absorption spectra are represented as $L(\hbar\Omega) \propto I(\hbar\Omega)[\hbar\Omega]^{-1}$. The advantage of such a representation is that the energy of Frank-Condon transitions can be directly derived from the maxima of the absorption and emission spectra.

Some typical room-temperature luminescence and absorption spectra of GSAG: Ce^{3+} at various pressures are shown in Fig. 2. The absorption and emission bands both shift to lower energy with pressure. The emission spectra have been deconvoluted into two Gaussian bands, which correspond to two transitions from the $5d(1)$ excited state to the lower ${}^2F_{5/2}$ and ${}^2F_{7/2}$ states. We observed an increase in the $5d(1) \rightarrow {}^2F_{7/2}$ emission intensity with increasing pressure. A similar effect of pressure is also observed in the study of YAG: Ce^{3+} .¹² In addition, the relative contribution from the $5d(1) \rightarrow {}^2F_{7/2}$ transition to the total emission in GSAG: Ce^{3+} was smaller than that in YAG: Ce^{3+} . Although these effects are experimentally evident, their origin is unclear and they need further detailed investigations. One possible reason for them is due to a pressure-induced change in the relative transition probability of the two emission transitions.

The peak energies and bandwidths of the absorption and emission bands as a function of pressure are presented in Figs. 3(a) and 3(b). From Fig. 3(a), we note that the peak energies of the two emission bands vary linearly with pressure. The shift rates are collected in Table I. The spin-orbit split ${}^2F_{5/2} - {}^2F_{7/2}$ energy (Δ) of Ce^{3+} in GSAG at ambient pressure is about 2090 cm^{-1} and exhibited a decrease at a rate of about $-0.8 \text{ cm}^{-1}/\text{kbar}$. Similarly, a decrease in Δ was also observed for the YAG: Ce^{3+} system.¹² This is due to a pressure-induced reduction of the spin-orbit coupling within the $4f$ electronic configuration. The effect of diminishing of the spin-orbit coupling was also observed and reported for Pr^{3+} -doped materials.¹⁴ In terms of the pressure dependence of the emission bandwidths, GSAG: Ce^{3+} exhibited a decrease, whereas YAG: Ce^{3+} exhibited an increase.¹²

More interestingly, we observed a larger shift in the absorption band than that in the two emission bands with pres-

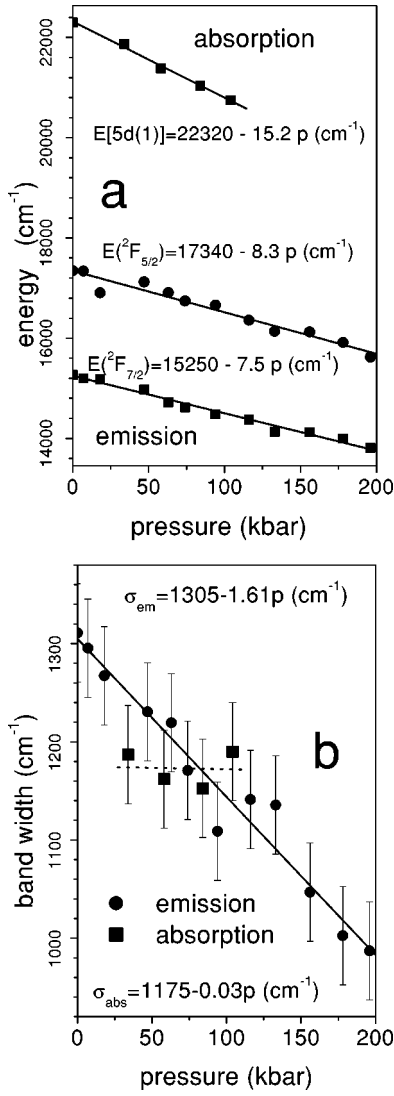


FIG. 3. Emission and absorption peak energies (a) and band-widths (b) as a function of pressure. Solid and dashed lines represent data for linear least-squares fits. In (a) the experimental error bars are not shown because their values are smaller than the size of the symbols.

sure [Fig. 3(a)]. This implies that the energetic separation between the absorption and emission band peaks is diminished upon pressurization. Within the configurational coordinate model [Fig. 1(b)], this separation can be given in a simple form:

TABLE I. Experimental data for the peak energies and pressure shifts of absorption and emission bands and values for the calculated parameters for Ce^{3+} in GSAG and YAG. $n=5$ was used for the calculations. Data included for YAG: Ce^{3+} have been obtained under the assumption that the pressure shift for the absorption band is the same as that for the emission bands.

	E_{depr} (cm^{-1})	E_{em} (cm^{-1})	dE_{em}/dp ($\text{cm}^{-1}/\text{kbar}$)	E_{abs} (cm^{-1})	dE_{abs}/dp ($\text{cm}^{-1}/\text{kbar}$)	B_0 (kbar)	K_Q	γK_R
GSAG	27000	17340 ± 100	-8.3 ± 0.5	22320 ± 100	-15.2 ± 0.7	1916 (Ref. 16)	0.65 ± 0.1	2.66 ± 0.4
YAG	27570	15250 ± 100	-7.5 ± 0.5	21750 ± 100	-12.5 ± 0.7	1870 (Ref. 15)	0.51 ± 0.1	1.02 ± 0.3
		19100 ± 100	-12.5 ± 0.7					
		17560 ± 100	-11.8 ± 0.7					

$$E_{abs} = E_{em} + 2S\hbar\omega. \quad (2)$$

Thus, using Eq. (2) we can directly find a pressure-induced reduction in the electron-lattice coupling and the coupling energy (or the lattice relaxation energy) shifts with pressure at a rate of $d(S\hbar\omega)/dP = 1/2[dE_{abs}/dP - dE_{em}/dP] = -3.5 \text{ cm}^{-1}/\text{kbar}$ for the $5d(1) \leftrightarrow ^2F_{5/2}$ transition.

III. DISCUSSION

In analyzing the peak energies of the emission and absorption bands and the lattice relaxation energy, we have used the configurational coordinate model and a harmonic approximation for the lattice potentials in the ground state (g , here corresponding to $^2F_{5/2}$ of Ce^{3+}) and the excited state [e , here corresponding to $5d(1)$ of Ce^{3+}] [Fig. 1(b)] to predict their energies [$E_g(Q)$ and $E_e(Q)$]

$$E_{g,e}(Q) = E_{g,e}^0 + \frac{1}{2}k_{g,e}(Q - Q_0)^2 + V_{g,e}(Q - Q_0), \quad (3)$$

where E_g^0 and E_e^0 are the pure electronic energies of the ground and excited states, respectively. Their difference $E_e^0 - E_g^0$ is equal to the difference between the $^2F_{5/2}$ state and the $5d^1$ (2D) state of the free Ce^{3+} ion additionally diminished by E_{depr} given by Eq. (1). k_g and k_e are the force constants for the ground and excited states, respectively. V_g and V_e are the electron-lattice coupling constants for the ground and excited states, respectively. Q_0 is a reference constant representing an initial value of the configurational coordinate.

In the crystal-field approach, the coupling constants (V_g and V_e) are expressed as

$$V_{g,e} = \left\langle \varphi_{g,e} \left| \frac{dU_{cr}(Q)}{dQ} \right| \varphi_{g,e} \right\rangle \approx \frac{d}{dQ} \langle \varphi_{g,e} | U_{cr}(Q) | \varphi_{g,e} \rangle, \quad (4)$$

where $U_{cr}(Q)$ is the crystal-field potential that is built by O^{2-} ligands surrounding Ce^{3+} . φ_e and φ_g are the electron wave functions for the excited and ground states, respectively. When we assume that the force constants for the ground and excited states are the same ($k_e = k_g = k$) and that the wave functions (φ_e and φ_g) are independent of Q within the adiabatic approximation, the crystal-field potential matrix elements in Eq. (4) can be written by $\langle \varphi_{g,e} | U_{cr}(Q) | \varphi_{g,e} \rangle = C_{g,e}/Q^n$, where $C_{g,e}$ are the coefficients depending on the

states and n is the n th term in the crystal-field potentials. Thus, in general, the coupling constants $V_{g,e}$ in Eq. (4) have a simple form:

$$V_{g,e} = -n \frac{C_{g,e}}{Q^{n+1}}. \quad (5)$$

In the point-charge model for the cubic crystal-field potential, only the $n=5$ term is a nonzero contribution from ligands. Since the $4f$ electron in Ce^{3+} is very well shielded by its outer $5s^2 5p$ valence electrons, the electron-lattice coupling in the ${}^2F_{7/2}$ and ${}^2F_{5/2}$ states is negligible with respect to the $5d$ electron that undergoes the strong influence from the oxygen ligands and we can thus use $V_{g=0}$ to obtain $S\hbar\omega = V_e^2/2k$.

To describe the variations of the absorption band peak energy (E_{abs}), the emission band energy (E_{em}), and the lattice relaxation energy ($S\hbar\omega$) with pressure, we take into account configurational coordinates as a function of pressure. Derivatives with respect to pressure can be written $dP = (dP/da)(da/dQ)dQ = (-3B_0/a)(da/dQ)dQ$, where B_0 is the bulk modulus of the host material and $a = \sqrt[3]{v}$. Here v is the cell volume. Further taking into account the crystal-field potential [$U_{cr}(Q)$] and the centroid shift [E_{cen} in Eq. (1)] as functions of Q^{-n} and $Q^{-n'}$, based on the point-charge model, respectively, we obtain

$$\frac{dE_{abs}}{dP} = \frac{K_Q}{3B_0} [nE_{cr} - n'E_{cen}] \quad (6)$$

and

$$K_Q = \frac{dQ}{Q} \bigg/ \frac{da}{a}. \quad (7)$$

Actually, K_Q is a microscopic parameter that measures a pressure-induced change in the local environment of Ce^{3+} relative to the host lattice. $K_Q=1$, $K_Q<1$, or $K_Q>1$ imply that the local compression is equal to, smaller than, or greater than the bulk compression, respectively. Using Eq. (6), we can obtain K_Q when dE_{abs}/dP is observed experimentally. For calculations we have assumed that $[-E_{cr} + (n'/n)E_{cen}] \approx [-E_{cr} + E_{cen}] = E_{depr}$. It is valid when $n = n'$. Actually since $n=5$ and $n'=6$ n'/n is greater than unity an absolute value of $-E_{cr} + n'/nE_{cen}$ is greater than E_{depr} . The error of approximation we have used depends on the ratio E_{cen}/E_{cr} . If it is of the order of unity (but it is probably smaller) the estimated K_Q is smaller by about 10% than it should be. In our opinion 10% is the accuracy of estimation of K_Q . We have found $K_Q=0.65$ for GSAG: Ce^{3+} and $K_Q=0.51$ for YAG: Ce^{3+} (Table I), which imply that the local compression is smaller than the bulk compression. Garcia-Revilla *et al.*¹⁷ have also reported $K_Q < 1$ for Ti-doped Al_2O_3 .

In a similar approach discussed above, the pressure dependence of the electron-lattice coupling energy ($S\hbar\omega$) is given by

$$\begin{aligned} \frac{dS\hbar\omega}{dP} &= S\hbar\omega \left[\frac{2}{V_e} \frac{dV_e}{dP} - \frac{1}{k} \frac{dk}{dP} \right] \\ &= \frac{S\hbar\omega}{3B_0} [2(n+1)K_Q - 6\gamma K_R], \end{aligned} \quad (8)$$

where γ is the Grüneisen parameter and has a following connection with the force constant

$$\frac{1}{k} \frac{dk}{da} = \frac{2}{\omega} \frac{d\omega}{da} = -\frac{6\gamma}{a} \quad (9)$$

and

$$K_R = \frac{dR}{R} \bigg/ \frac{da}{a}. \quad (10)$$

K_R is analogous to K_Q and another microscopic parameter that is, in fact, a relative measure of the influence of pressure on local vibration modes in the vicinity of $[\text{CeO}_8]^{13-}$ defect centers with respect to the influence of pressure on the lattice modes. Since Ce^{3+} as a defect center substitutionally occupies a Gd^{3+} site, K_R like K_Q also has three different cases: $K_R < 1$, $K_R = 1$, and $K_R > 1$. Moreno *et al.*¹⁸ and Marco de Lucas *et al.*¹⁹ have studied the dependence of zero-phonon line energy and Stokes shift on ion-ligand distance in perovskites and proposed a similar relation like Eq. (8) for describing changes of electron-lattice coupling. K_R concerns the compression of the interionic distance (R) between Ce^{3+} and its nearest neighboring oxygen ions as well as its next-nearest neighboring cations such as Al^{3+} in YAG and Al^{3+} and/or Sc^{3+} in GSAG. Thus, K_R unlike K_Q is probably close to unity.

We define γK_R as γ_{loc} that can be considered as the local Grüneisen parameter of Ce^{3+} . When the electron-lattice coupling energy ($S\hbar\omega$) is obtained experimentally, using Eq. (8) we can compute γ_{loc} . Values for γ_{loc} of Ce^{3+} in GSAG: Ce^{3+} and YAG: Ce^{3+} were obtained and are included in Table I. We found the local Grüneisen parameter $\gamma_{loc} = 2.66$ for GSAG: Ce^{3+} and 1.12 for YAG: Ce^{3+} . The bulk Grüneisen parameters for garnets are reported to be between 1 and 2.²⁰ The local and bulk Grüneisen parameters are very similar in both the host lattices.

The electron-lattice coupling in GSAG: Ce^{3+} was observed to be weakened considerably due to compression and its coupling energy decreases at a rate of $-3.5 \text{ cm}^{-1}/\text{kbar}$. Pressure-induced narrowing of the emission bands observed in GSAG: Ce^{3+} [Figs. 2 and 3(b)] gave a consistency. However, the emission bandwidths of YAG: Ce^{3+} were observed to increase with pressure¹² and this implies that the electron-lattice coupling may have an opposite pressure behavior. It is interesting to note that the electron-lattice coupling energy ($S\hbar\omega$) in GSAG: Ce^{3+} at ambient pressure is almost as twice as that in YAG: Ce^{3+} . According to Eq. (8), a smaller $S\hbar\omega$ should have a weaker pressure dependence. GSAG has a larger cell parameter (1.243 nm) than YAG (1.200 nm).^{21,22} The pressure-induced reduction in the electron-lattice coupling energy in the larger GSAG lattice is stronger than that in the smaller YAG lattice. If such a relation between the

electron-lattice coupling and the cell parameter holds valid, $[2(n+1)K_Q - 6\gamma K_R] < 0$ works for a class of materials, in our present case, garnets.

In our present work, we have considered an effective local vibrational mode that can be described by the single configurational coordinate model. This corresponds to the a_1 symmetry breathing mode. Another vibrational mode that can be active in the electron-lattice interaction taking place in the $5d(1)$ emitting state in a cubic or nearly cubic field is a two-dimensional ϵ mode leading to Jahn-Teller effects via $\epsilon \times E$. When the E state of $5d$ split by a local lower symmetry than the cubic, an evident energy minimum occurs in the two-dimensional configurational space. In this case, one can always consider the cross-section area in which the energy is described still by Eq. (3). The consideration of the ϵ mode instead of the a_1 mode included in the analysis of the electron-lattice coupling actually has no influence on the second term in Eq. (8). $S\hbar\omega$ for the ϵ mode is now called the Jahn-Teller stabilization energy and Eq. (5) is still valid for dealing with the coupling constant V , but n is 3 rather than 5.²³ When $n=3$ is used, the local Grüneisen parameter is smaller by 15% in GSAG:Ce³⁺ and 30% in YAG:Ce³⁺. Assuming that 30% is the accuracy of our calculations the

Jahn-Teller contributions are considered within the errors of our estimation for the local Grüneisen parameter.

IV. CONCLUSIONS

We have performed high-pressure absorption and luminescence studies in Ce³⁺-doped GSAG and observed a strong pressure-induced reduction in the electron-lattice coupling. In the context of the single configurational coordinate model and the conventional crystal-field model, a quantitative analysis of pressure-induced redshifts in the peak energies of absorption and emission bands has resulted in the information about the local compression modulus and local Grüneisen parameter. Our present simple model can be generalized and applied, in principle, to other material systems that occupy electronic interconfigurational transitions.

ACKNOWLEDGMENTS

This work was supported by the Polish State Committee for Scientific Research under Grant No. 2P03 B057 23, by the U.S. National Science Foundation under Grant No. DMR-0107802, and also partially by the U.S. Department of Energy under Cooperative Agreement No. DE-FC08-01NV14049 with the University of Nevada Las Vegas.

-
- ¹S. Kück, Appl. Phys. B: Lasers Opt. **72**, 515 (2001).
²M. Balcerzyk, Z. Gontarz, M. Moszynski, and M. Kapusta, J. Lumin. **87-89**, 963 (2000).
³P. Dorenbos, J. Lumin. **91**, 155 (2000).
⁴*Phosphor Handbook*, edited by S. Shionoya and W.M. Yen (CRC Press, New York, 1989).
⁵G. Randolph, Laser Focus World **31**, 121 (1995).
⁶J. Hecht, Laser Focus World **31**, 53 (1995).
⁷M.J. Padgett and M.H. Dunn, Laser Focus World **30**, 69 (1994).
⁸B. Henderson and R.H. Bartram, *Crystal-field Engineering of Solid State Laser Materials* (Cambridge University Press, Cambridge, 2000).
⁹C.A. Morrison, J. Chem. Phys. **72**, 1001 (1980).
¹⁰C.W. Struck and W.H. Fonger, *Understanding Luminescence Spectra and Efficiency Using W_p and Related Functions* (Springer-Verlag, Berlin, 1991).
¹¹W.B. Yen, J. Lumin. **83-84**, 399 (1999).
¹²M. Grinberg, J. Barzowska, and T. Tsuboi, Radiat. Eff. Defects Solids **158**, 39 (2003).
¹³Y.R. Shen, R.S. Kumar, M.S. Pravica, and M.F. Nicol (unpublished).
¹⁴C. Bungenstock, Th. Troster, and W.B. Holzapfel, Phys. Rev. B **62**, 7945 (2000).
¹⁵V.F. Kitaeva, E.V. Zharikov, and I.L. Chisty, Phys. Status Solidi A **92**, 475 (1985).
¹⁶Y.N. Xu, W.Y. Ching, and B.K. Briceken, Phys. Rev. B **61**, 1817 (2000).
¹⁷S. Garcia-Revilla, F. Rodriguez, R. Valiente, and M. Pollnau, J. Phys.: Condens. Matter **14**, 447 (2002).
¹⁸M. Moreno, M.T. Barriuso, and J.A. Arambury, J. Phys.: Condens. Matter **4**, 9481 (1992).
¹⁹M.C. Marco de Lucas, F. Rodriguez, and M. Moreno, Phys. Rev. B **50**, 2760 (1994).
²⁰M. Dutoit, J. Appl. Phys. **45**, 2836 (1974).
²¹M. Kokta, J. Solid State Chem. **8**, 357 (1973).
²²F. Euler and J.A. Bruce, Acta Crystallogr. **19**, 961 (1965).
²³C.A. Bates and J.P. Bentley, J. Phys. C **2**, 1947 (1969).